Optical Engineering

OpticalEngineering.SPIEDigitalLibrary.org

Dual-line optical waveguides in Cu:KNSBN crystal fabricated by direct femtosecond laser writing

Weijie Nie
Javier R. Vázquez de Aldana
Feng Chen

SPIE.

Dual-line optical waveguides in Cu:KNSBN crystal fabricated by direct femtosecond laser writing

Weijie Nie,[a] Javier R. Vázquez de Aldana,[b] and Feng Chen[a,*]
[a]Shandong University, School of Physics, Jinan 250100, China
[b]Universidad de Salamanca, Laser Microprocessing Group, Departamento Física Aplicada, Salamanca 37008, Spain

Abstract. We report on dual-line waveguides fabricated by direct femtosecond laser writing in Cu:KNSBN crystal. Two different sizes have been designed with the separation between lines of 20 and 30 μm, respectively. The detailed structure of the dual-line waveguide has been imaged by means of micro-Raman analysis, indicating that the microstructure of the Cu:KNSBN crystal has no significant change after direct femtosecond laser writing. The dual-line waveguides support single-mode guidance along both transverse electric and transverse magnetic polarization at the wavelengths of 632.8 and 1064 nm, and show insensitivity to polarization of light. We suggest the potential application of the laser-written Cu:KNSBN waveguides as new integrated optical devices. [DOI: 10.1117/1.OE.54.9.097106]

Keywords: optical waveguides; femtosecond laser writing; Cu:KNSBN crystals.

Paper 150875 received Jun. 28, 2015; accepted for publication Aug. 21, 2015; published online Sep. 21, 2015.

1 Introduction

Photonic devices based on the photorefractive effect have tremendous application prospects in holographic storage, self-adaptive optics, coherent detection, optical computing, optical communication, image processing, and so on.[1–3] For the photorefractive effect, potassium sodium strontium barium niobate $[(K_{0.5}Na_{0.5})_{0.2}(Sr_{0.75}Ba_{0.25})_{0.9}Nb_2O_6$; KNSBN] is one of the well-known candidates due to its large electro-optic coefficient ($r_{33} \sim 270 \times 10^{-12}$ m/V and $r_{51} \sim 400 \times 10^{-12}$ m/V), which is much larger than that of some conventional nonlinear crystals such as lithium niobate ($LiNbO_3$) and lithium tantalite ($LiTaO_3$).[4–6] In addition, compared with strontium barium niobate (SBN), KNSBN has a relatively higher Curie temperature (120°C to 250°C) and easier preparation.[7] When active ions (i.e., copper) with certain concentrations were doped, controllable and intriguing photorefractive or ferroelectric properties could be produced in this crystal,[8] which could be desirable in some photonic devices such as guided-wave optical devices. Optical waveguides, which are the basic elements in integrated photonics, can confine light in small volumes, reaching relatively high optical intensities inside the structure.[9] As a result, a high performance of photorefractive properties could be easily obtained in waveguides. Benefiting from these advantages, optical waveguides in Cu:KNSBN can have a number of potential applications such as low-cost optical devices in commercial optical systems, when combined with some other components, e.g., fibers or laser diodes.[1,10–12]

Waveguides in electro-optic crystals for photorefractive applications could be fabricated by several techniques, including focused ion-beam writing,[13] ion/proton exchange,[14] ion implantation,[15,16] and femtosecond laser inscription.[17,18] Ion implantation was first applied to achieve planar waveguides in Cu:KNSBN.[19] Since 1996, femtosecond laser inscription has emerged as a powerful technique to realize three-dimensional waveguiding structures in diverse transparent materials.[20] During the processing, the energy of the femtosecond pulses is absorbed in the substrates through nonlinear processes (i.e., two-photon or multiphoton absorption)[21,22] followed by avalanche ionization. Because of this feature, femtosecond laser pulses create either positive or negative refractive index changes through the combined effect of the nature of the material and laser parameters such as repetition rate, wavelength, polarization, pulse energy, focusing conditions, and scanning speed.[23–26] Depending on the type of material modification that is induced with the laser, different approaches can be followed to fabricate waveguides. When the so-called type I modification is induced (weak damage), a refractive index increase typically occurs at the focal volume, producing a guiding region in this area. A single laser scan or multiple parallel scans lead to the fabrication of a waveguide.[27] For higher powers, severe damage is produced (type II modification) with a refractive index decrease in the damage tracks. However, due to the stress-induced during the laser–matter interaction, a refractive index increase may appear near the tracks.[28] Waveguides with type II modification are usually fabricated by inscribing two parallel laser damage tracks (so-called dual-line technique), thus increasing the magnitude of the refractive index modification in the area between both tracks, and that is the region where the waveguide is produced. Another approach based on reduced refractive index modifications is the depressed-cladding waveguides[29–31] (sometimes called type III waveguides), in which the waveguide core (not modified) is surrounded by a large number of laser tracks (refractive index decrease) that define the cladding. Compared with waveguides based on type I modification, the bulk features in the stress-induced waveguides may not be affected significantly and it is possible to achieve guidance for the two laser polarizations in the stress-induced waveguides. Furthermore, the modal feature of dual-line

*Address all correspondence to: Feng Chen, E-mail: drfchen@sdu.edu.cn

waveguides can support single-mode guidance and the waveguide region has a smaller size compared to depressed cladding waveguides.[21,32]

In this work, we report on the fabrication of the dual-line waveguides in Cu:KNSBN crystal by direct femtosecond laser writing with no significant change in the microstructure, which guide transverse electric (TE) and transverse magnetic (TM) polarized modes and show good transmission properties at the wavelengths of 632.8 and 1064 nm.

2 Experiments Details

The Cu:KNSBN crystal (doped with 0.04 wt.% CuO) was cut with the dimensions of $6(c) \times 4(a) \times 2(a)$ mm^3 and optically polished. Figure 1(a) shows the process of the femtosecond laser inscription, which was carried out using the facility at University of Salamanca, Spain. The laser source is a Ti:Sapphire amplifier (Spitfire, Spectra Physics) that delivers linearly polarized pulses with a temporal duration of 120 fs, a central wavelength of 795 nm, and a low-repetition-rate of 1 kHz. The maximum available pulse energy is 1 mJ, and it was controlled by a calibrated neutral density filter placed after a set of half-wave plates and a linear polarizing cube. The laser irradiation was controlled with a mechanical shutter. The laser beam was focused by a 40× microscope objective lens at 150 μm beneath one of the sample surfaces (with sizes of 6×4 mm^2) and the focal spot would be around 1.8 μm. The sample was placed on a computer-controlled XYZ micropositioning stage.

To obtain the optimum waveguide fabrication parameters, different pulse energies and scan velocities were tested. Figure 1(b) is the cross-sectional microscope images of femtosecond laser inscribed tracks produced with a constant velocity of 50 μm/s and different pulse energies of 0.2, 0.4, 0.6, 0.8, 1.6 μJ (from left to right). It is found that, as the pulse energy increases, the damage track becomes more intense and grows slightly in length. For pulse energies of 0.8 μJ or above, the track split into two or more parts which is probably due to multiple refocusing of the femtosecond laser pulse in the filamentation process.[33] The multiple tracks separate further as the energy is increased. The effect of the scanning velocity is shown in Fig. 1(c) for a pulse energy of 0.8 μJ (velocities of 200, 100, 50, 25, 10 μm/s, from left to right): larger scanning velocities (less spatial overlap between consecutive pulses) lead to less damaged tracks. In order to fabricate the dual-line waveguides, it is desirable to use large pulse energy in order to produce a great compression of the crystalline lattice in the surroundings of the tracks: however, the effect of track splitting is undesirable because it leads to complex stress fields producing a separated guiding region. Thus, we selected a pulse energy of 0.8 μJ as the threshold value for the appearance of track splitting. Two scanning velocities, 25 and 50 μm/s, were used in the fabrication.

Under these circumstances, several parallel tracks were inscribed by the laser along the c-axis of the crystal forming the type II waveguides. The separations between two lines were chosen to be 20 and 30 μm. Table 1 shows all the details of the fabricated dual-line waveguides, including the scanning velocity of the femtosecond laser, actual measured separation distances, and the number of exhibited microphotographs.

To investigate the microstructure change induced by the femtosecond laser inscription, the μ-Raman spectra of the sample were measured by a confocal micro-Raman spectrometer (Horiba/JobinYvon HR800). The exciting laser beam had a wavelength of 473 nm with a diameter of the focused spot (size of the detected region) of ~1 μm.

The near-field modal distributions of the dual-line waveguides were performed by employing a typical end-face coupling system. The schematic of the experimental arrangement is shown in Fig. 2. Two linearly polarized lasers with different wavelengths (632.8 and 1064 nm) focused with a microscope objective in one end-face of the waveguides were used for characterization. The modal profile at the output of

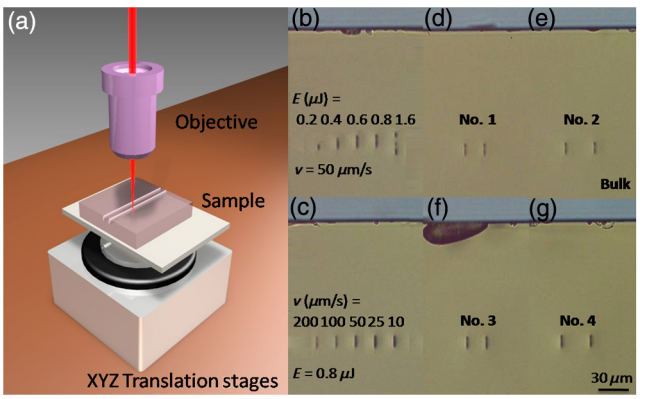

Fig. 1 (a) The schematic plot of a femtosecond laser-written dual-line structure in the Cu:KNSBN crystal. Transmission microscope images of the tracks produced in Cu:KNSBN crystal by 120-fs pulses showing the effect of (b) the pulse energy and (c) the scanning velocity. In the image (b), the pulse energy from left to right was set to 0.2, 0.4, 0.6, 0.8, 1.6 μJ with the constant velocity of 50 μm/s along the c-direction. In the image (c), the scanning velocity from left to right was set to 200, 100, 50, 20, 10 μm/s with the same pulse energy of 0.8 μJ. (d)–(g) Optical microscope images of the cross sections of dual-line waveguides Nos. 1 to 4, respectively.

Table 1 The parameters of fabricated waveguides (pulse energy 0.8 μJ).

Number	Scan velocity	Separation	Figure exhibition
No. 1	50 μm/s	20 μm	Fig. 1(d)
No. 2	50 μm/s	30 μm	Fig. 1(e)
No. 3	25 μm/s	20 μm	Fig. 1(f)
No. 4	25 μm/s	30 μm	Fig. 1(g)

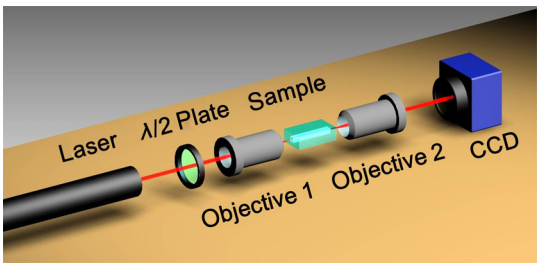

Fig. 2 Schematic of the end-face coupling arrangement used to investigate the near-field intensity distributions of the Cu:KNSBN waveguides.

the waveguide was imaged onto a CCD by another objective lens. Based on the above arrangement, the NA of the waveguide was measured by rotating a cubic glass to adjust the position of the incident coupling light for the purpose of getting the maximum value of the refractive index change of the dual-line waveguide. Moreover, the propagation losses of the structures were estimated and determined by directly measuring the input light power and output power of the transmitted light taking the Fresnel reflection in the interface of the waveguide end face and the air into account.

3 Results and Discussion

Figure 3 demonstrates the μ-Raman spectra of both bulk and the core of waveguide No. 4, which was similar to the other waveguides. From comparison, the peak positions and widths of the μ-Raman spectra for the waveguide region exhibit no obvious change, while the intensity of the peak is enhanced about 6.8%. The small modification is assumed to be induced by the stress effect between tracks formed by femtosecond laser inscription. Results of the μ-Raman spectra in the sample indicate the absence of a significant lattice structure change in the waveguide region, consequently the performance of photorefractive properties is expected to be well preserved.

Figures 4 and 5 exhibit the measured near-field modal distributions (fundamental modes) of the dual-line waveguides Nos. 1 to 4 for the TE and TM polarizations (i.e., TE_{00} and TM_{00}) by the CCD at the wavelengths of 632.8 and 1064 nm, respectively. During the experiment, it is hard to excite higher-order modes of the waveguides, which means the main energy of the light fields is confined in the fundamental modes. The full-width-half-maximum of the near-field intensity distribution of the waveguides in the X and Y directions were listed in the Table 2. To obtain the polarization-independent effects of the transmission, the all-angle light guidance along the transverse plane was measured. The performance of all waveguides is similar at 632.8 and 1064 nm: as an example, the all-angle light guidance of waveguide No. 4 at 1064 nm is shown in Fig. 6. It is found that the output power is nearly constant for any polarization of the input light (i.e., approximately polarization-independent):

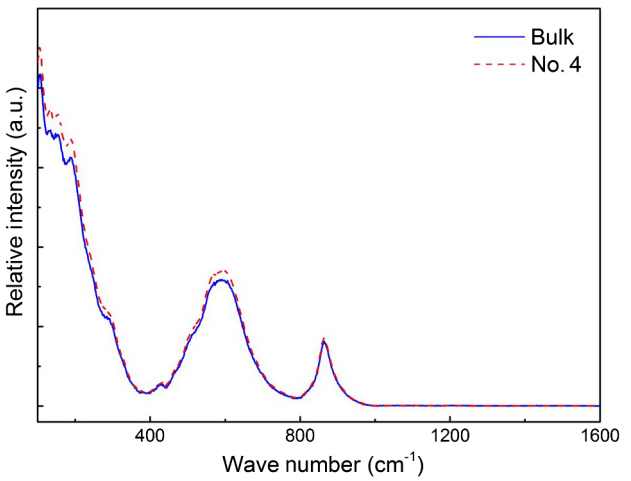

Fig. 3 Confocal micro-Raman spectrum obtained from the waveguide No. 4 (red) and the bulk (blue) of the Cu:KNSBN.

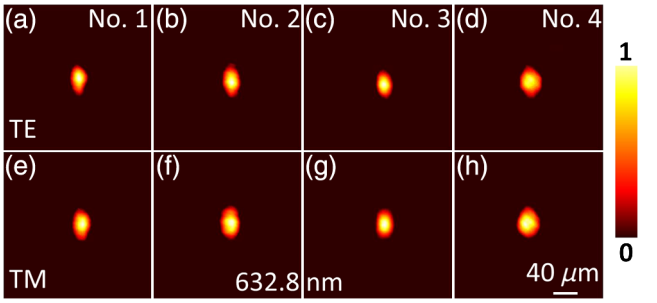

Fig. 4 Measured near-field intensity distribution of dual-line waveguides Nos. 1 to 4 for: (a)–(d) TE_{00} and (e)–(h) TM_{00} polarizations at 632.8 nm.

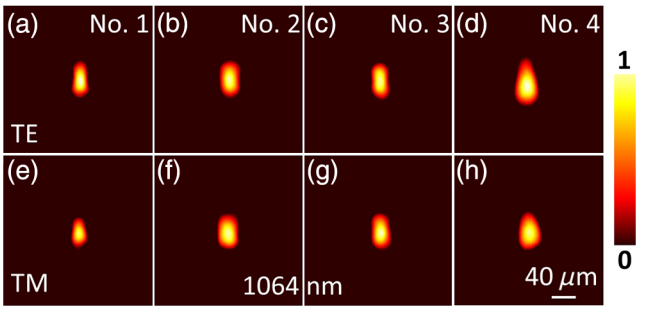

Fig. 5 Measured near-field intensity distribution of dual-line waveguides Nos. 1 to 4 for: (a)–(d) TE_{00} and (e)–(h) TM_{00} polarizations at 1064 nm.

Table 2 The full-width-half-maximum (FWHM) of the dual-line waveguides.

Waveguide		FWHM (μm) at 632.8 nm		FWHM (μm) at 1064 nm	
		X	***Y***	***X***	***Y***
No. 1	TE	10.45	20.10	8.74	17.45
	TM	11.05	21.25	8.87	15.82
No. 2	TE	15.41	22.80	13.60	20.19
	TM	19.62	26.77	14.96	20.76
No. 3	TE	13.38	21.51	10.10	19.07
	TM	12.94	21.94	9.66	17.73
No. 4	TE	20.72	25.20	14.67	18.61
	TM	20.69	27.63	14.98	25.94

it is an obvious advantage over the reported dual-line waveguides fabricated in other crystals (e.g., Nd:YAG and Nd:GGG) that only support the TM guided modes.[21]

In order to get the refractive index contrasts between the damage lines and the waveguide region, the numerical aperture method introduced by Siebenmorgen et al.[34] is utilized by assuming a step-index profile of the femtosecond laser modification. The maximum refractive index modification can be roughly estimated with the equation

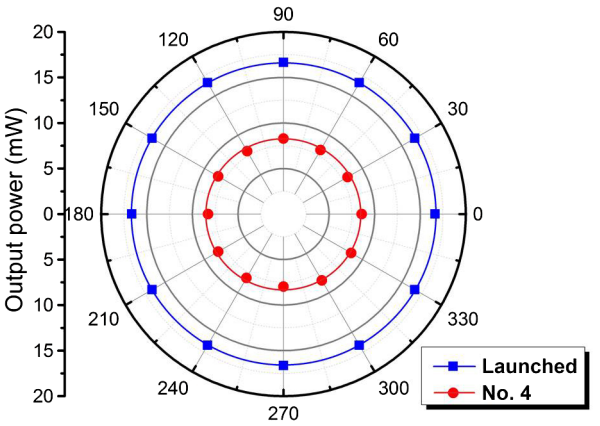

Fig. 6 Output power as a function of all-angle light transmission with the same launched power of dual-line Cu:KNSBN waveguide No. 4 at 1064 nm.

$$\Delta n \approx \frac{\sin^2 \theta_m}{2n}, \tag{1}$$

where θ_m is the maximum incident angular deflection at which no change of the transmitted power occurred, and n is the refractive index of the bulk at the corresponding wavelength. In this work, the calculated index changes for waveguides Nos. 1 to 4 at 632.8 nm are 2.8×10^{-3}, 1.5×10^{-3}, 3.9×10^{-3}, 2.3×10^{-3}, respectively.

Afterward, the two-dimensional (2-D) refractive index profiles of the dual-line waveguides were reconstructed with the obtained Δn by using the near-field method.[35] The mode profile has been found analytically starting from Maxwell's equations. The numerically calculated field profile has been smoothed using the digital filter and the smoothed field has been used to calculate the index profile. The index change of each point can be given by

$$\Delta n_i = \sqrt{n_s - f\frac{1}{k^2 A}\nabla_t^2 A} - n_s, \tag{2}$$

where n_s is the substrate index value, k is the propagation constant in the medium, and A is the normalized electric field intensity. The relation of A and f is

$$A = \sqrt{\frac{I}{I_{\max}}} f. \tag{3}$$

Figure 7(a) demonstrates the reconstructed 2-D refractive index profile of dual-line waveguide No. 4 along the TM polarization (at 632.8 nm). According to the reconstructed 2-D refractive index profile, the light propagation at that wavelength in the waveguide was simulated by using the software Rsoft®, based on the finite difference beam propagation method.[36,37] Figure 7(b) depicts the calculated modal distribution of waveguide No. 4 corresponding to the reconstructed 2-D refractive index profile in Fig. 7(a), which is in good agreement with the experimental data of Fig. 4(h). Therefore, the reconstructed refractive index profile of the dual-line waveguide is proved to be reasonable.

Based on the end-face coupling system, propagation losses of the waveguides in Cu:KNSBN crystal, an essential

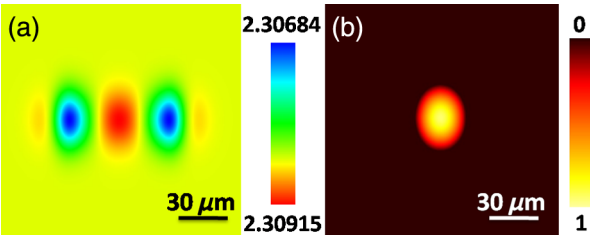

Fig. 7 (a) Reconstructed two-dimensional refractive index profile at the cross section and (b) calculated modal profile of dual-line Cu:KNSBN waveguide No. 4 of transverse magnetic (TM) polarization at 632.8 nm.

Table 3 The losses α (dB/cm) of the dual-line waveguides.

	α (dB/cm) at 632.8 nm		α (dB/cm) at 1064 nm	
Waveguide	TE	TM	TE	TM
No. 1	2.23	2.08	1.30	1.18
No. 2	3.43	3.04	1.79	1.69
No. 3	1.67	1.54	0.94	0.84
No. 4	2.98	2.89	1.41	1.24

factor in the performance of waveguides, were estimated. The obtained values for TM (TE) modes at 632.8 and 1064 nm are listed in Table 3. According to the data of the propagation losses α, it is concluded that $\alpha_3 < \alpha_1 < \alpha_4 < \alpha_2$. Waveguides No. 1 and No. 3 with a track separation of 20 μm are superior to No. 2 and No. 4 of 30 μm, which shows that the separation of 30 μm is too wide to confine the light with good transmission properties in the waveguide region. On the other hand, with the same separation, the waveguides fabricated with a scan velocity of 25 μm/s have lower losses than those of 50 μm/s, i.e., $\alpha_3 < \alpha_1$ and $\alpha_4 < \alpha_2$, which may be due to the larger refractive index increase (better confinement) induced at low velocities.

As has been shown, for a fixed pulse energy, the waveguide performances are very sensitive to the other main fabrication parameters: track separation and scanning velocity. In summary, the optimum performance in Cu:KNSBN dual-line waveguides is achieved with the smaller scannning velocity (25 μm/s) and minimum track separation (20 μm). However, the isotropic behavior of the waveguide in terms of polarization confinement and the well-confined mode behavior is observed in all the studied waveguides.

4 Summary

In conclusion, we have reported dual-line waveguides in Cu:KNSBN crystal fabricated by a femtosecond laser with different separations. The guiding properties and propagation losses at 632.8 and 1064 nm were investigated, showing good guidance along both the TE and TM polarizations. The good performances of the waveguides (with no significant change in the lattice microstructure) and the polarization insensitivity suggest the produced dual-line waveguides in

Cu:KNSBN crystal as potential integrated photonic devices in compact optical systems.

Acknowledgments

This work was supported by the National Natural Science Foundation of China (Grant No. 11274203) and Ministerio de Economía y Competitividad under Project FIS2013-44174-P, Spain.

References

1. R. Singh, R. A. Yadav, and D. P. Singh, "Comparative study of the signal-to-noise ratio and gain in photorefractive materials," *J. Russ. Laser Res.* **34**(6), 509–514 (2013).
2. P. Gunter and J. P. Huignard, *Photorefractive Materials and their Application*, Springer, Berlin (1988).
3. G. Roosen, J. P. Huignard, and M. Cronin-Golomb, "Photorefractive materials, effects, and devices introduction," *J. Opt. Soc. Am. B* **7**(12), 2242 (1990).
4. F. Chen et al., "Characterization of optical planar waveguide in Ce: KNSBN crystal formed by triple-energy helium ion implantation," *Appl. Surf. Sci.* **253**(7), 3589–3594 (2007).
5. X. Sun, F. Yao, and Y. Pei, "The study of bridge phase conjugation in photorefractive Tb: Cu: KNSBN crystal,"*J. Mod. Opt.* **51**(13), 1889–1897 (2004)
6. D. Sun et al., "Growth and self-pumped phase conjugation of Ce-doped $KNa(Sr_{0.61}Ba_{0.39})_{0.9}Nb_2O_6$ crystal," *J. Appl. Phys.* **70**(1), 33–36 (1991).
7. F. Chen et al., "Planar waveguides in Ce:SBN and Cu:KNSBN crystals by 6.0 MeV B^{3+} ion implantation," *Appl. Surf. Sci.* **202**(1–2), 86–91 (2002).
8. Y. Tomita and S. Matsushima, "Photorefractive beam coupling between orthogonally polarized light beams by linear dichroism in Cu-doped potassium sodium strontium barium niobate," *J. Opt. Soc. Am. B* **16**(1), 111–116 (1999).
9. G. Lifante, *Integrated Photonics: Fundamentals*, Wiley, England (2003).
10. A. Dazzi et al., "High performance of two-wave mixing in a $BaTiO_3$ waveguide realized by He^+ implantation," *J. Opt. Soc. Am. B* **16**(11), 1915–1920 (1999).
11. D. Kip et al., "Photorefractive properties of ion-implanted waveguides in strontium barium niobate crystals," *Appl. Phys. B* **65**(4–5), 511–516 (1997).
12. D. Fluck et al., "Cerenkov-type second-harmonic generation in $KNbO_3$ channel waveguides," *IEEE J. Quantum Electron.* **32**(6), 905–916 (1996).
13. R. He et al., "Focused ion-beam writing of channel waveguides in BGO crystal for telecommunication bands," *Opt. Eng.* **54**(5), 057108 (2015).
14. E. Flores-Romero et al., "Planar waveguide lasers by proton implantation in Nd:YAG crystals," *Opt. Express* **12**(10), 2264–2269 (2004).
15. F. Chen, "Micro- and sub-micrometric waveguiding structures in optical crystals produced by ion beams for photonic applications," *Laser Photonics Rev.* **6**(5), 622–640 (2012).
16. I. Bányász et al., "Leaky mode suppression in planar optical waveguides written in $Er:TeO_2$-WO_3 glass and CaF_2 crystal via double energy implantation with MeV N^+ ions," *Nucl. Instrum. Methods B* **326**, 81–85 (2014).
17. C. Grivas et al., "Tunable, continuous-wave Ti:sapphire channel waveguide lasers written by femtosecond and picosecond laser pulses," *Opt. Lett.* **37**(22), 4630–4633 (2012).
18. G. C. Righini and A. Chiappini, "Glass optical waveguides: a review of fabrication techniques," *Opt. Eng.* **53**(7), 071819 (2014).
19. F. Lu et al., "Planar optical waveguide in Cu-doped potassium sodium strontium barium niobate crystal formed by mega-electron-volt He-ion implantation," *Opt. Lett.* **22**(3), 163–165 (1997).
20. I. M. Davis et al., "Writing waveguides in glass with a femtosecond laser," *Opt. Lett.* **21**(21), 1729–1731 (1996).
21. F. Chen and J. R. V. de Aldana, "Optical waveguides in crystalline dielectric materials produced by femtosecond-laser micromachining," *Laser Photonics Rev.* **8**(2), 251–275 (2014).
22. B. C. Stuart et al., "Nanosecond-to-femtosecond laser-induced breakdown in dielectrics," *Phys. Rev. B* **53**(4), 1749–1761 (1996).
23. I. Burghoff et al., "Structural properties of femtosecond laser-induced modifications in $LiNbO_3$," *Appl. Phys. A* **86**(2), 165–170 (2006).
24. S. M. Eaton et al., "Transition from thermal diffusion to heat accumulation in high repetition rate femtosecond laser writing of buried optical waveguides," *Opt. Express* **16**(13), 9443–9458 (2008).
25. I. Will et al., "Optical properties of waveguides fabricated in fused silica by femtosecond laser pulses," *Appl. Opt.* **41**(21), 4360–4364 (2002).
26. M. Ams, G. D. Marshall, and M. J. Withford, "Study of the influence of femtosecond laser polarization on direct writing of waveguides," *Opt. Express* **14**(26), 13158–13163 (2006).
27. A. Ródenas and A. Kar, "High-contrast step-index waveguides in borate nonlinear laser crystals by 3D laser writing," *Opt. Express* **19**(18), 17820–17833 (2011).
28. I. Burghoff, S. Nolte, and A. Tunnermann, "Origins of waveguiding in femtosecond laser-structured $LiNbO_3$," *Appl. Phys. A* **89**(1), 127–132 (2007).
29. Y. Ren et al., "Mid-infrared waveguide lasers in rare-earth-doped YAG," *Opt. Lett.* **37**(16), 3339–3341 (2012).
30. G. Salamu et al., "Cladding waveguides realized in Nd:YAG ceramic by direct femtosecond-laser writing with a helical movement technique," *Opt. Mater. Express* **4**(4), 790–797 (2014).
31. W. Nie et al., "Dual-wavelength waveguide lasers at 1064 and 1079 nm in Nd:YAP crystal by direct femtosecond laser writing," *Opt. Lett.* **40**(10), 2437–2440 (2015).
32. H. Liu et al., "Waveguiding microstructures in Nd:YAG with cladding and inner dual-line configuration produced by femtosecond laser inscription," *Opt. Mater.* **39**, 125–129 (2015).
33. A. Couarion and A. Mysyrowicz, "Femtosecond filamentation in transparent media," *Phys. Rep.* **441**, 47–189 (2007).
34. I. Siebenmorgen et al., "Femtosecond laser written stress-induced $Nd:Y_3Al_5O_{12}$ (Nd:YAG) channel waveguide laser," *Appl. Phys. B* **97**(2), 251–255 (2009).
35. I. Mansour and F. Caccavale, "An improved procedure to calculate the refractive index profile from the measured near-field intensity," *J. Lightwave Technol.* **14**(3), 423–428 (1996).
36. RSoft Design Group, "BeamPROP," http://www.rsoftdesign.com (2007).
37. D. Yevick and W. Bardyszewiski, "Correspondence of variational finite-difference (relaxation) and imaginary-distance propagation methods for modal analysis," *Opt. Lett.* **17**(5), 329–330 (1992).

Weijie Nie received her BS degree from Shandong Normal University, Jinan, China, in 2014. Currently, she is working toward her PhD at Shandong University, Jinan, China. Her current research interests include fabrication of optical waveguides in optical crystals by using femtosecond laser writing.

Javier R. Vázquez de Aldana received his Bachelor of Science degree (1997) and his PhD (2001) from the University Salamanca, Spain. Currently, he is an associate professor of the Science Faculty, University of Salamanca, Spain. His research activity is focused on the interaction of intense femtosecond pulses with materials and its application to fabrication of photonic devices. He is a member of the Laser Microprocessing Research Group and is also responsible for the Microprocessing Laboratory of the Spanish Laser Facility CLPU.

Feng Chen is a professor at Shandong University, China. He received his PhD from Shandong University in 2002. He was with Clausthal University of Technology, Germany, from 2003 to 2005, as a Humboldt research fellow. He has published more than 200 papers in peer-reviewed journals. He is a fellow of the Institute of Physics, UK, a senior member of the OSA, and a member of SPIE. He also serves as an associate editor of *Optical Engineering*.